AIAA JOURNAL
Vol. 31, No. 5, May 1993

Study of Supersonic Intersection Flowfield at Modified Wing-Body Junctions

B. Lakshmanan* and S. N. Tiwari†
Old Dominion University, Norfolk, Virginia 23529

The problem of supersonic flow control using fillets and sweep for a wing-body junction has been investigated numerically using a three-dimensional Navier-Stokes code, which employs the MacCormack's time-split finite volume technique. An elliptic grid generation technique with direct control over spacing has been developed for constructing the grid at a filleted wing-body junction. The computed results for pressure distribution, particle paths, and limiting streamlines on the flat plate and fin surface for a swept fin show a decrease in the peak pressure on the fin leading edge and in the extent of the separated flow region. Moreover, the results for filleted juncture clearly show that the flow streamline patterns lose much of their vortical character with proper filleting. It has been demonstrated that fillets with a radius of three-and-one-half times the fin leading-edge diameter are required to weaken the vorticity in the horseshoe vortex by a factor of three for the Mach number and Reynolds number considered in the present study.

Nomenclature

a	= speed of sound
CFL	= Courant-Friedrichs-Lewy number
C_f	= skin friction coefficient
D	= diameter of the fin
E	= total energy per unit mass
e_i	= specific internal energy, $T/\gamma(\gamma - 1)$
H	= height of the fin
i	= index in ξ direction
j	= index in η direction
k	= index in ζ direction
L_ξ, L_η, L_ζ	= finite difference operators in ξ, η, and ζ directions
M	= Mach number
Pr_l	= laminar Prandtl number
Pr_t	= turbulent Prandtl number
p	= static pressure
R	= radius of the fillet at the juncture
T	= static temperature
t	= time
q	= vector of conserved variables
u	= velocity component in x direction
v	= velocity component in y direction
w	= velocity component in z direction
x, y, z	= global coordinates
x_0	= distance from the flat plate leading edge to fin leading edge
γ	= ratio of specific heats, c_p/c_v
Δt	= time step used in the split operators
δ	= boundary-layer thickness
Λ	= fin sweep angle
λ	= second coefficient of viscosity, $-\frac{2}{3}\mu$
μ	= dynamic molecular viscosity
ξ, η, ζ	= body oriented coordinates
ρ	= density
σ	= safety factor in the stability criteria equation
ω	= vorticity magnitude

Subscripts

e	= evaluated at the boundary-layer edge corresponding to $u/u_e = 0.995$
$t2$	= measured using a pitot tube
∞	= evaluated in freestream conditions

Introduction

MANEUVERING flight vehicles operating from subsonic to supersonic speeds encounter three-dimensional separation at several intersecting surfaces such as wing-fuselage and wing-pylon junctions and air-breathing engine inlets. The flow originating at the intersecting surfaces depicts complex flow patterns that may significantly affect the performance of the aircraft. The major effects are increased pressure and heat transfer level in the vicinity of the intersections and loss of control effectiveness due to flow separation. Thus, the prediction and control of complex three-dimensional separated flows is of vital importance to the aircraft designer. A variety of simplified geometrical configurations have been studied to understand the physical aspects of three-dimensional separated flows. Some of these include 1) a sharp fin mounted on a flat plate, 2) a blunt fin mounted on a flat plate, 3) a swept compression corner, and 4) a semicone affixed to a flat plate.

In this paper we consider the high-speed flow past a blunt fin/flat plate junction (Fig. 1), which is a typical example of junction flow. This type of flowfield is characterized by the presence of shock waves in the flowfield in addition to the vortical structures observed in low-speed flows.[1,2] The detached bow shock formed ahead of the fin induces a strong adverse pressure gradient to the flat plate boundary layer. This gradient results in a separated flow region composed of horseshoe vortices downstream of the separation point and a lambda-type shock in the plane of symmetry. Immediately downstream of this vortex, there appears to be one or more vortices, depending on the geometric and flow parameters. The reversed flow in the vortices is constantly replenished by the separated stream flow and spirals downstream very rapidly. The compressed separated flow ahead of the fin accelerates to supersonic velocities in escaping around the fin to regions of low pressure. A strong corner vortex originates at the fin root and spreads out as it follows the fin root downstream. In addition, the separation shock emanating from the separated flow region impinges on the bow shock and is reflected. A shear layer starts at the triple point and separates the subsonic flow from a jet of supersonic flow. The flow in the supersonic jet passes through several oblique shocks (see the enlarged view of the supersonic jet in Fig. 1) and is com-

Received Feb. 10, 1992; revision received Aug. 6, 1992; accepted for publication Aug. 18, 1992.

*Research Associate, Department of Mechanical Engineering and Mechanics. Member AIAA.

†Eminent Professor, Department of Mechanical Engineering and Mechanics. Associate Fellow AIAA.

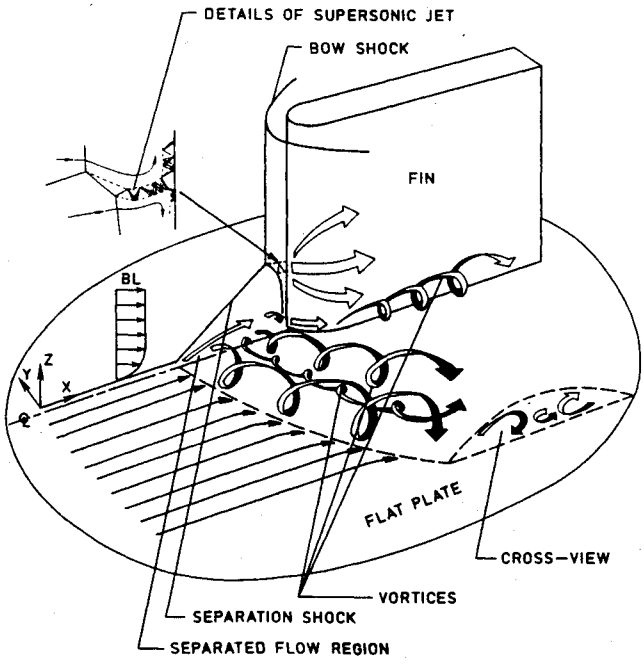

Fig. 1 Simplified flow structure at the blunt fin/flat plate junction.

pressed nearly isentropically leading to extremely large pressure and high heat transfer locally on the fin leading edge and adjoining regions in the immediate vicinity of the fin root.

Three-dimensional shock wave and boundary-layer interacting flows, induced by circular cylinders or hemispherically blunted fins in supersonic boundary layers, have been the subject of extensive experimental and analytical research over the past few years. A juncture flow problem was investigated experimentally by Sedney[3] using a flow visualization technique. The main objective of the experiment was to correlate the separation distance as a function of Mach number, Reynolds number, and obstacle dimensions. Experiments have been carried out by previous investigators on a class of related problems to study the effect of transition properties on diameter of the fin,[4-13] height of the protuberance,[4,6,9] incoming boundary-layer thickness,[4,8,10,11] and Reynolds number.[4,6,11,14,15] Most of the experimental studies have concentrated on obtaining the flow characteristics in the plane of symmetry. Dolling et al.,[12,13] however, have examined the spanwise extent of the disturbed flowfield. Price and Stallings[6] measured the wall pressure distributions at selected spanwise locations for a wide range of fin diameter, sweep angle, and height of the protuberance. Young et al.[16] experimentally investigated strong interactions between fin generated shock waves and laminar and turbulent boundary layers for Mach 3 and 5 flows. Özcan and Holt[17] recently investigated the high-speed laminar flow characteristics of a circular cylinder on a flat plate using the oil flow visualization technique. Hung and Kordulla[18] developed a general finite volume algorithm to study the blunt fin induced shock wave/turbulent boundary-layer interaction whereas Horstman[19] and Knight[20] studied the sharp fin induced shock wave/turbulent boundary-layer interaction problem.

Because of the complexity of the problem, most of the experimental studies have concentrated on obtaining the flow characteristics in the plane of symmetry and selected spanwise locations. With the availability of vector processors such as the Cray II and Cyber 205, solutions of three-dimensional Navier-Stokes equations for realistic configurations are now possible. The specific objective of the present study is to control the supersonic intersection flowfields through filleting and sweep. Attention is specifically directed toward modifying the supersonic wing-body junction with circular and continuous fillets and fin sweep. The ultimate goal of the research effort is to predict the optimal fillet radius and fin sweep to weaken the horseshoe vortex and thereby achieve a smooth flow with minimum distortion.

Physical Model and Theoretical Formulation

The physical model and coordinate system for the flow past a blunt fin/flat plate junction are shown in Fig. 1. As mentioned in the Introduction, a high-speed flow past such configurations results in a complex flow structure with viscous-inviscid and shock-shock interactions. The essential features of the flowfield are shown in Fig. 1 in a simplified form.

The theoretical formulation of the problem starts with the nondimensional form of the compressible three-dimensional Navier-Stokes equations cast in the generalized body oriented coordinate system. Specifically, the integral form of the Navier-Stokes equations without external body forces and source terms is used, and this is expressed as[21]

$$\frac{\partial}{\partial t}\int_v q\,dv + \int_s (qu + b)\cdot n\,ds = 0$$

$$q = (\rho,\ \rho u,\ \rho v,\ \rho w,\ \rho E)^T$$

$$E = e_i + \tfrac{1}{2}(u^2 + v^2 + w^2)$$

$$b = (b_\rho,\ b_m,\ b_e)^T$$

$$b_\rho = 0$$

$$b_m = pI + M_\infty Re_D^{-1}\underline{\tau}$$

$$\underline{\tau} = -\lambda \mathrm{div} u I - \mu[(\mathrm{grad}\ u) + (\mathrm{grad}\ u)^T]$$

$$b_e = -\gamma M_\infty (Re_D Pr)^{-1}\mu\ \mathrm{grad}\ e_i + pu + M_\infty Re_D^{-1}\underline{\tau}\cdot u \quad (1)$$

The nondimensionalization of the governing equations is carried out by normalizing the Cartesian velocity components (u, v, w) by the sound speed a_∞, the density ρ by ρ_∞, the specific internal energy e_i and the total internal energy E by a_∞^2, and p by $\rho_\infty a_\infty^2$. The viscosity coefficients λ and μ are normalized by the molecular viscosity μ_∞. The governing equations are further supplemented by the following equations of state:

$$p = (1/\gamma)\rho T, \qquad e_i = T/\gamma(\gamma - 1), \qquad a^2 = T \quad (2)$$

where T is normalized by the freestream static temperature.

The preceding system of equations is valid for both laminar and turbulent flows by replacing the molecular transport coefficients with their turbulent counter parts, i.e.,

$$\mu = \mu_l + \mu_t \quad (3a)$$

$$\frac{\mu}{Pr} = \frac{\mu_l}{Pr_l} + \frac{\mu_t}{Pr_t} \quad (3b)$$

where μ_t represents the turbulent eddy viscosity. The molecular dynamic viscosity is evaluated using Sutherland's law of viscosity.

Turbulence Modeling

An important conclusion of the numerical study of Knight et al.[22] was that the overall structure of the three-dimensional sharp fin interaction flowfield was insensitive to the turbulence model employed, except within a small portion of the boundary layer adjacent to the flat plate surface. They used two different turbulence models, the algebraic eddy viscosity model of Baldwin and Lomax[23] and the k-ϵ model. This method resulted in significant differences in computed turbulent eddy viscosity profiles. However, the velocity profiles computed by both models were in close agreement. Similar conclusions were reached by Hung and Bunning[21] in the simulation of a blunt fin interaction flowfield. It was demonstrated that the overall structure of the horseshoe vortex was inviscid dominated and was only weakly dependent on the incoming

boundary-layer thickness. Based on these observations and because of the computational simplicity, it was decided that the Baldwin and Lomax[23] turbulence model would be used in the present study. However, no attempt was made to account for the history and amplification of turbulence intensity after a sudden strong compression through a shock wave. The use of more realistic or complex turbulence models is left for future studies.

Thin-Layer Approximation

For high-Reynolds-number flows, the effects of viscosity are confined to a thin layer near the wall boundary. In this region, the viscous terms in the normal direction dominate the flow and the viscous effects along the body direction are usually small and negligible. The development of the thin-layer approximation by Baldwin and Lomax[23] is based on this concept, with the retention of the unsteady and all of the inviscid terms of the Navier-Stokes equations. The extension of thin-layer approximation to two directions was demonstrated in a previous study of supersonic flow over an axial comer.[24] Here, the concept is extended to the case of thin layers in all three directions for a general coordinate system. All of the viscous terms associated with the cross derivatives are neglected compared to normal second-derivative terms. The neglected cross derivatives near the wall can be of the same order of magnitude as the normal derivatives, but the flow there contains comparatively very low momentum fluid. Hence, such an approximation will not significantly influence the flow at the junction. The use of thin-layer approximation greatly simplifies evaluation of the viscous terms and allows easy vectorization of the algorithm.

Boundary and Initial Conditions

The fin is assumed to be semi-infinite in height and length. Consequently, zeroth order extrapolations can be applied in these directions. The fin is assumed to be at zero angle of attack, and a symmetry boundary condition is imposed at the plane of symmetry. The wall is assumed impermeable, and no-slip and no-penetration boundary conditions are applied. The wall conditions are also assumed to be adiabatic, and the pressure has a zero gradient normal to the wall.

The outer boundary $J = J_{\max}$ is set far away to avoid any influence on the interaction region. Since the flow is boundary-layer-like at these locations, theoretically one can specify a boundary-layer profile on the flat plate at each axial location along the outer boundary. These profiles can be generated easily from their corresponding points of a flow over an isolated flat plate using a boundary-layer code. In the present study, the region of interest is assumed small compared with the length of the flat plate generating the incoming boundary-layer profile. Hence, the variation of the boundary-layer profile at the outer boundary is assumed small and is neglected. Therefore, one predetermined boundary-layer profile is prescribed for all x locations along the outer boundary.

The initial conditions required to initiate the computation are obtained by simply propagating the specified boundary profiles at $J = J_{\max}$ everywhere in the computational domain. To correct the erroneous occurrence of negative density in the flowfield and thereby allow a large CFL number to be used during the startup phase, the blunt body starting condition as suggested in Ref. 18 is used.

Method of Solution

Grid Generation

As shown in Fig. 2, a modified elliptic grid generation technique[25] with direct control over the grid spacing is used to generate the mesh at a filleted wing-body junction and swept fin/flat plate junction. The equation of the super ellipse $(x/a)^n + (y/b)^n = 1$ is used to generate the grid for the filleted junction. The grid lines are clustered near the plate and fin surfaces as well as near the connecting surface region using a geometric grid stretching formula to provide adequate resolution of the viscous effects. The three-dimensional grid employed in the flow computation is generated by rotating the grid in the plane of symmetry about the fin leading edge. Because the flow is assumed to be symmetric, only one-half of the flow is computed.

Computational Procedures

The computer program used in this study is coded for a three-dimensional generalized body-fitted coordinate system. As such, various geometries can be handled by the code. The code employs the MacCormack's explicit predictor-corrector method[26] using the time-split finite volume technique.

The time splitting reduces the complex three-dimensional operators into a sequence of three one-dimensional operators. Thus, the split operator contains the spatial flux derivatives in only one direction. The finite difference formulation in terms of the split operators can be expressed as

$$\hat{q}^{n+2} = L_\eta(\Delta t)L_\zeta(\Delta t)L_\xi(2\Delta t)L_\zeta(\Delta t)L_\eta(\Delta t)\hat{q}^n \tag{4}$$

Each split operator consists of a predictor and a corrector step. During a specific numerical sweep, the inviscid fluxes are forward differenced in the prediction sequence and backward differenced in the correction step. The viscous fluxes are always centrally differenced. The composite numerical method is second-order accurate in both time and space, is conditionally stable, and requires no scalar or block tridiagonal inversions. Artificial smoothing terms are explicitly added to the fluxes to stabilize the numerical scheme when computing flows with strong shocks. Since an explicit scheme is utilized in the present study, the time step used for integrating the governing equations is restricted by the stability criteria. Because of the complex nature of the compressible Navier-Stokes equations, it is not possible to obtain a closed-form stability expression for the MacCormack scheme applied to these equations. However, the following empirical formula can normally be employed:

$$\Delta t \le \sigma(\Delta t)_{\text{CFL}} \tag{5}$$

In Eq. (5), σ is the safety factor ($\simeq 0.9$) for viscous problems and $(\Delta t)_{\text{CFL}}$ is the inviscid CFL condition given by

$$(\Delta t)_{\text{CFL}} \le \left(\frac{|u|}{\Delta x} + \frac{|v|}{\Delta y} + \frac{|w|}{\Delta z} + a\sqrt{\frac{1}{(\Delta x)^2} + \frac{1}{(\Delta y)^2} + \frac{1}{(\Delta z)^2}}\right)^{-1} \tag{6}$$

Results and Discussion

Numerical solutions for laminar and turbulent flows were obtained for several cases that are discussed in detail in Refs. 1 and 2. For the sake of brevity, only selected results of the grid refinement study carried out for the laminar flow past a blunt fin/flat plate junction have been included in Fig. 3. To check the numerical accuracy of the solution procedure, the flowfield results were obtained using three different meshes

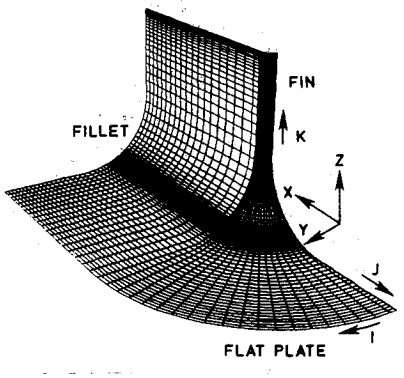

Fig. 2 Grid structure at a filleted wing-body junction.

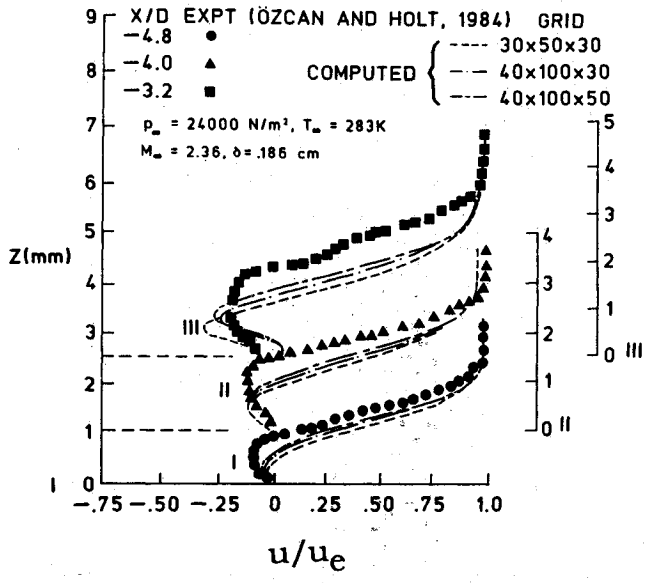

Fig. 3 Effect of grid refinement on the computed axial velocity profile for a laminar flow past a blunt fin/flat plate junction.

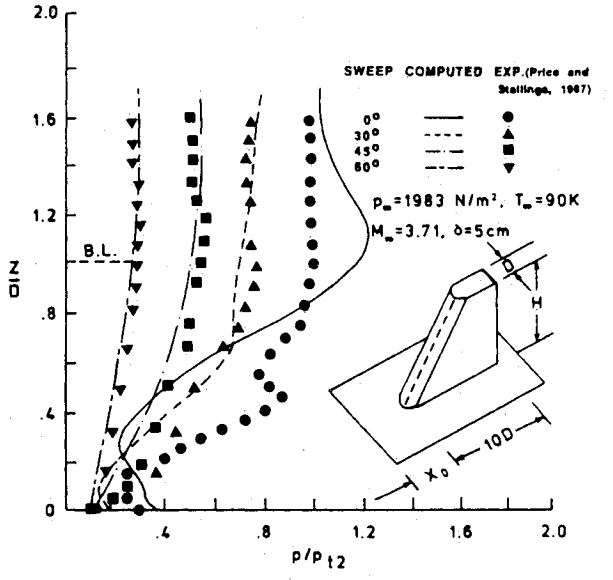

Fig. 4 Comparison of pressure distribution on the fin leading edge for various fin sweeps.

$30 \times 50 \times 30$, $40 \times 100 \times 30$, and $40 \times 100 \times 50$. It was found that the velocity profiles displayed some sensitivity to grid refinement (Fig. 3) but the overall topological structure of the flow was unchanged. In addition, the most upstream extent of separation did not show any significant change with grid refinement. Because the extent of turbulent separation ahead of blunt fins is much shorter and the horseshoe vortex flowfield is inviscid dominated, it was decided to use a $40 \times 45 \times 45$ mesh for all computations in the present work. With this grid, all pertinent flow features are adequately resolved.

For the turbulent flow past a swept fin, the results are compared with experimental measurement of Price and Stallings[6] in a high Reynolds number flow. After this validation, the results of filleted fin-induced interactions are compared with the results of the blunt fin interactions.

Turbulent Flow Past a Swept Fin

For the case of swept fin induced shock wave/boundary-layer interaction, comparative results were obtained for the following specific conditions:

$M_\infty = 3.71$, $T_{o\infty} = 339$ K, $P_{o\infty} = 203{,}055$ N/m^2

$\delta = D = 5$ cm, $H = 35$ cm, $\Lambda = 0$ deg to 60 deg

The pressure distributions along the fin stagnation line are compared in Fig. 4 for various fin sweep angles. The pressure is nondimensionalized by the total pitot pressure behind the bow shock, p_{t2}. The agreement between the numerical results and the experimental data is seen to be good except for the zero sweep blunt fin, where the level of pressure is underpredicted in the boundary layer and overpredicted in the inviscid region. The experimental measurements[6] indicated that "an irregular pressure distribution does in fact occur and the location of peak pressure within the boundary layer is a function of sweep as well as Mach number. Lack of data in the region near the wall prevents identifying a peak for any of the other models with this diameter. A more complete experimental investigation would have to be performed to define, for a certainty, the flow model responsible for this irregular pressure distribution." A close examination of the figure reveals that as the fin sweep angle increases, the magnitude of peak pressure decreases considerably from 1.2 to 0.2. The variation in pressure from the position of peak to minimum is substantially reduced by increasing fin sweeps. The increase in pressure in the direction towards the plate surface from the position of minimum is not seen for fin sweep angles greater than 30 deg.

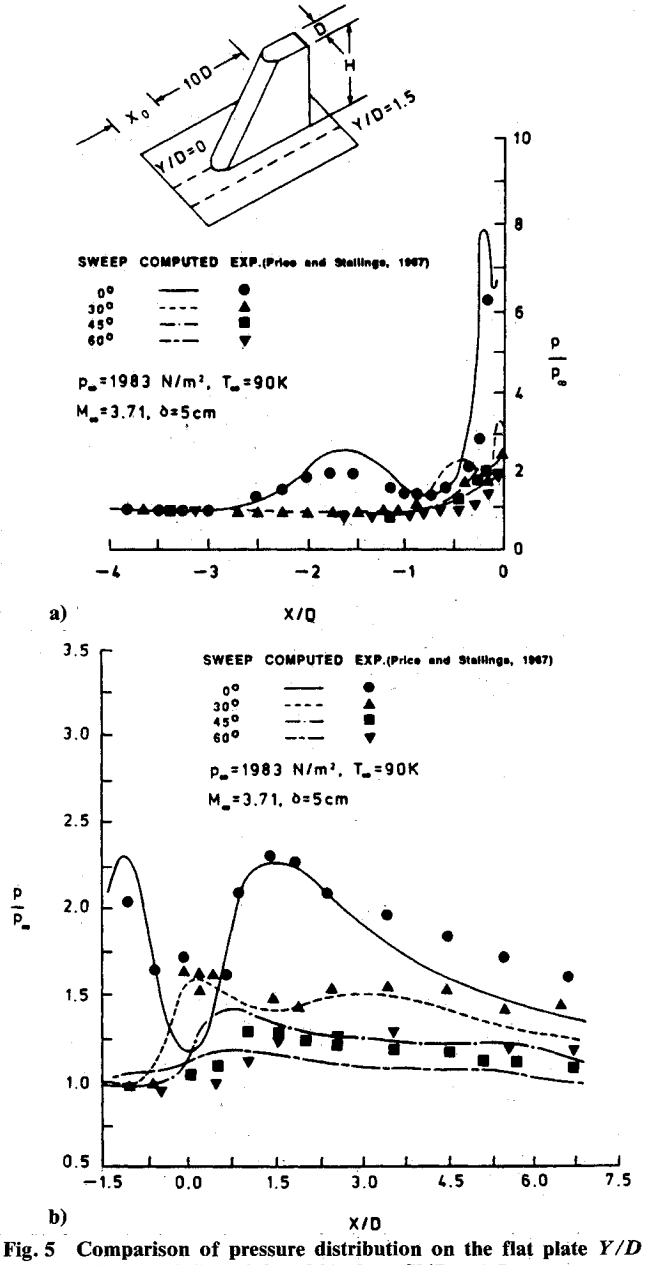

Fig. 5 Comparison of pressure distribution on the flat plate Y/D = const: a) along $Y/D = 0.0$ and b) along $Y/D = 1.5$.

The comparison of pressure distribution on the flat plate along the line of symmetry ($Y/D = 0$) and off the line of symmetry ($Y/D = 1.5$) is illustrated in Fig. 5. Again the agreement is very good. The code is able to simulate all of the pertinent flow features such as upstream influence, pressure rise due to flow separation from the flat plate, and double peaks in pressure off the line of symmetry. Further examination of the results reveal a low-pressure region between the first peak in pressure and the final compression region along the line of symmetry (Fig. 5a). The low-pressure region observed is due to the existence of a reversed high-speed flow region. However, for sweep angles greater than 30 deg the low-pressure region is not seen. The disappearance of the low-pressure trough region for high fin sweep angles demonstrates the weakening of the main horseshoe vortex with the sweep. Further examination of the results illustrates that the sweep considerably decreases the upstream influence. The appearance of double peaks in pressure on the flat plate away from the plane of symmetry (Fig. 5b) can be explained by following the conclusions reached by Hung and Bunning.[21] Off the line of symmetry, the second peak in pressure is a result of the expansion as the flow passes over the blunt fin. The low-pressure region between the two peaks in pressure is caused by the high velocity near the plate under the core of the vortex. This high velocity and low pressure under the core of a vortex is a typical phenomenon called the ground effect of a vortex. Such phenomena occur usually in separated cross flows but are seldom explained.

The computed limiting streamline patterns are shown in Fig. 6 for blunt and 60-deg swept fins. The separation and reattachment lines are also marked. The foot trace left by the horseshoe vortex as the flow goes around the fin is clearly observed in the area bounded by the separation and reattachment line. It is apparent that the spanwise influence exerted by the horseshoe vortex on the juncture flow is considerably

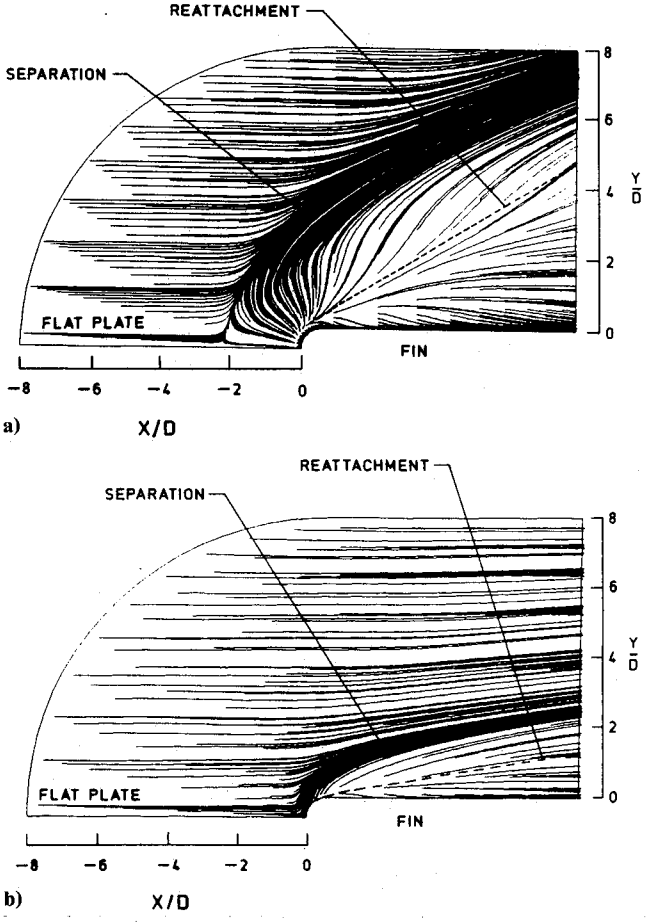

Fig. 6 Computed streamline patterns on the flat plate: a) sweep = 0 deg and b) sweep = 60 deg.

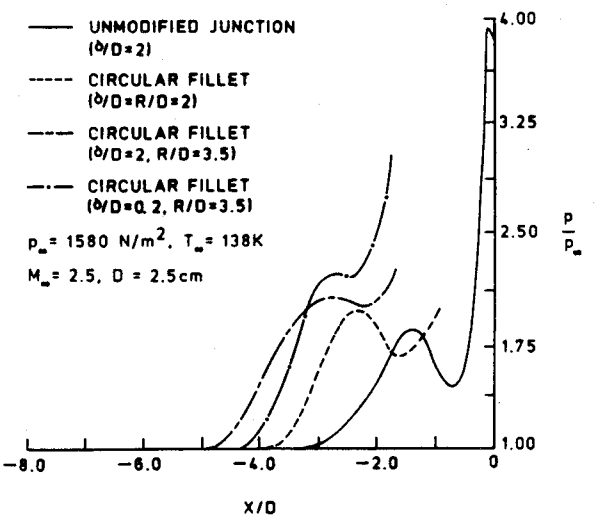

Fig. 7 Pressure distribution on the flat plate for various types of junctions.

reduced for high sweep angles. In particular, at a sweep angle of $\Lambda = 60$ deg, the flow beyond the spanwise location $Y/D = 3.0$ (Fig. 6b) is unaffected from the juncture effect. However, in the case of the blunt fin the extent of the disturbed flow persists up to $Y/D = 6.0$ (Fig. 6a).

Turbulent Flow Past a Filleted Fin

For the case of turbulent flow past a filleted fin/flat plate junction, results were obtained corresponding to the following conditions:

$$M_\infty = 2.4, \qquad T_{o\infty} = 312 \text{ K}, \qquad P_{o\infty} = 27{,}000 \text{ N/M}^2$$

$$\delta = 5 \text{ cm}, \qquad D = 2.5 \text{ cm}, \qquad H = 20 \text{ cm}$$

$$R = 5 \text{ and } 9 \text{ cm}$$

The pressure distributions along the line of symmetry are compared in Fig. 7 for various types of junctions. It is clear that the pressure distributions due to filleted junctions are greater in magnitude than those measured at corresponding points with the unmodified junction. An interesting feature of the surface pressure distribution in the plane of symmetry is the "trough" in pressure that occurs ahead of the leading edge in all of the junctions considered in the present study. As mentioned before, the low-pressure region is caused by a high velocity under the core of the horseshoe vortex. With the fillet, this trough is less pronounced and occurs further upstream from the fin leading edge, suggesting that the horseshoe vortex has considerably diminished in strength. Moreover, with an increase in fillet radius the separation point moves further upstream of the fin leading edge. The fillet does not completely eliminate leading-edge separation or the formation of a horseshoe vortex. Instead, it displaces the separated flow away from the fin surface in a manner that suggests it increases the effective radius of the nose of the fin. A similar trend in results was observed in a low-speed turbulent flow past filleted wing-body junctions.[27]

The computed vorticity contours in the plane of symmetry are shown in Fig. 8 for unmodified and modified junctions. Clearly, in the case of the modified junction, there is a factor of three reduction in the magnitude of vorticity in the core of the horseshoe vortex as compared with the unmodified junction. Furthermore, in the case of the modified junction, the vorticity contours are deformed and elongated as compared with the unmodified junction in which there is a concentration of vorticity at the center of the vortex. Because in the present work the mixing length model was used, it was not possible to

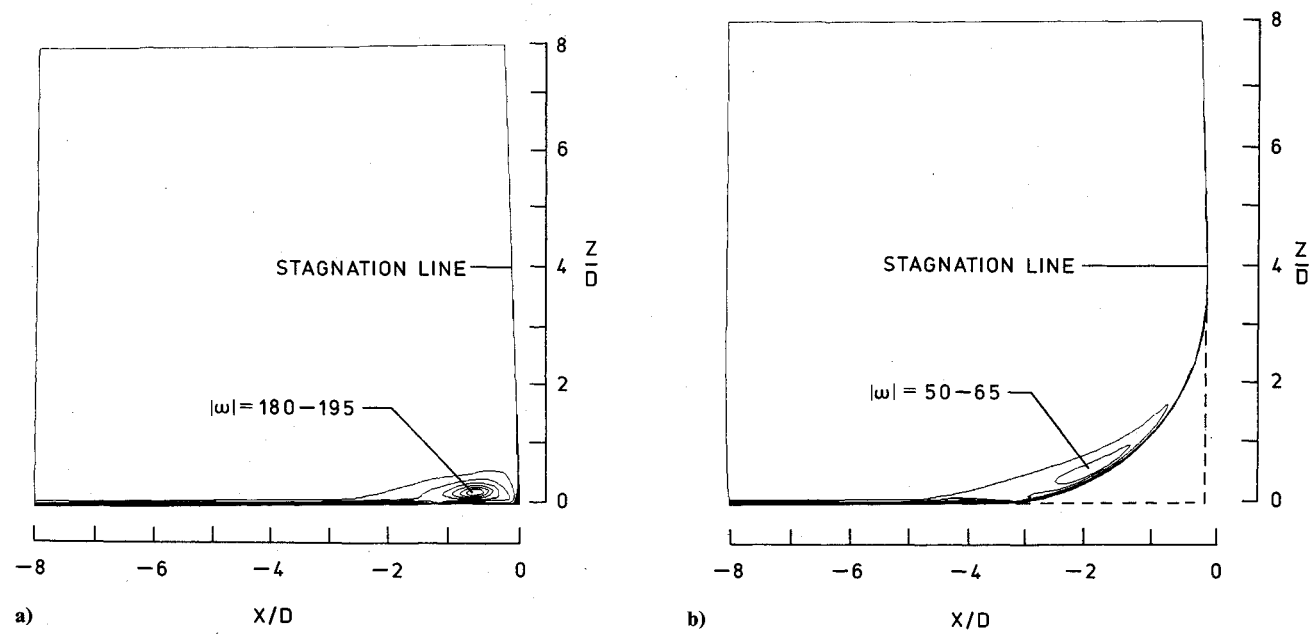

Fig. 8 Computed vorticity contours in the plane of symmetry for various types of junctions: a) unmodified junction ($\delta/D = 2$) and b) circular fillet ($\delta/D = 2$, $R/D = 3.5$).

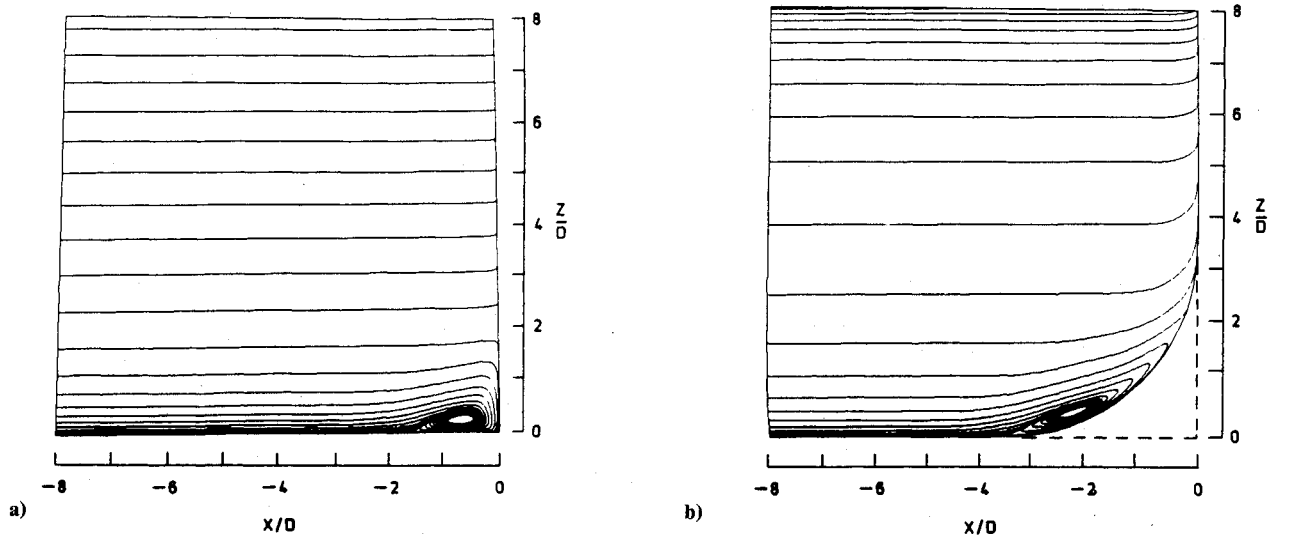

Fig. 9 Computed particle paths in the plane of symmetry for various types of junctions: a) unmodified junction ($\delta/D = 2$) and b) circular fillet ($\delta/D = 2$, $R/D = 3.5$).

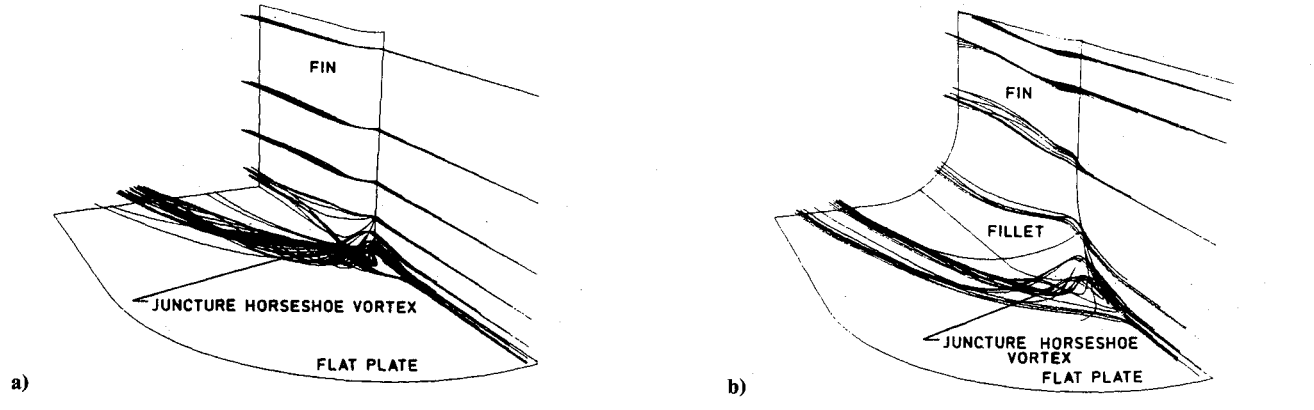

Fig. 10 Computed time-averaged streamlines for various types of junctions: a) unmodified junction ($\delta/D = 2$) and b) circular fillet ($\delta/D = 2$, $R/D = 3.5$).

compute the turbulence level at the junction. To evaluate the turbulence level one needs to use a k-ϵ model.

The computed particle paths in the plane of symmetry are shown in Fig. 9 for unmodified and modified junctions. The influence of filleting on the flow structure is apparent as compared to the unmodified junction. The particle paths demonstrate that the horseshoe vortex deforms and the flow streamlines within the boundary layer lose much of their vortical character with proper filleting (see also Fig. 10). Other results presented in Ref. 1 indicate that the separation on the fin surface due to the comer vortex is prevented completely in the case of the modified junction. The time-averaged streamlines are shown in Fig. 10 for unmodified and modified junctions employing circular fillets. Here the fluid particles are released at $I = 1$, $J = J_{max}$ along the same physical locations in the z direction to clearly show the global effect of fillets on the juncture flow. It is apparent that the released particles outside the boundary-layer region proceed undisturbed in both junctions. However, the particle trace within the boundary layer of the unmodified junction continues to roll up far downstream of the juncture as compared with the modified junction, in which the rollup is considerably reduced. These results demonstrate the improvements to the flow structure obtained by suitably modifying the junction and its effect on the helical vortex structure in supersonic flows.

Conclusions

The supersonic flow past a fin and flat plate junction is simulated numerically using a three-dimensional Navier-Stokes code. The results for swept fin induced shock wave/turbulent boundary-layer interaction are in good agreement with experimental measurements. Detailed information on the computed pressure distribution and limiting streamline pattern on the flat plate surface for the swept fin clearly shows a considerable decrease in the spanwise extent of the disturbed flow. The numerical study of filleted junctures demonstrates that it is possible to reduce the magnitude of vorticity in the horseshoe vortex by a factor of three with proper filleting. However, the leading-edge separation and formation of the horseshoe vortex could not be completely eliminated. Fillets with a radius of three-and-one-half times the fin leading-edge diameter are required to substantially weaken the usual necklace vortex interaction for the Mach number and Reynolds number considered in the present study.

Acknowledgments

This work was supposed by NASA Langley Research Center through Grant NAG1-530. The authors are indebted to D. M. Bushnell and M. Y. Hussaini of NASA Langley Research Center for originally suggesting the problem and providing many stimulating discussions during the course of this study. The authors would also like to thank C. M. Hung of NASA Ames Research Center for providing his three-dimensional Navier-Stokes code to perform some of the computations presented in this work.

References

[1]Lakshmanan, B., Tiwari, S. N., and Hussaini, M. Y., "Control of Supersonic Intersection Flowfields through Filleting and Sweep," *Proceedings of the First AIAA/ASME/SIAM/APS National Fluid Dynamics Congress,* Cincinnati, OH, July 1988, pp. 746–759.

[2]Lakshmanan, B., "Numerical Study of Three-Dimensional Separation and Flow Control at a Wing/Body Junction," Ph.D. Dissertation, Old Dominion Univ., Norfolk, VA, Aug. 1989.

[3]Sedney, R., "A Survey of the Effects of Small Protuberances on Boundary Layer Flows," *AIAA Journal,* Vol. 11, No. 6, 1973, pp. 782–792.

[4]Sedney, R., and Kitchens, C. W., Jr., "Separation Ahead of Protuberances in Supersonic Turbulent Boundary Layers," *AIAA Journal,* Vol. 15, No. 4, 1977, pp. 546–552.

[5]Voitenko, D. M., Zubkov, A. I., and Panov, Y. A., "Supersonic Gas Flow Past a Cylindrical Obstacle on a Plate," *Mehanika ZhidkostiiGaza,* Vol. 1, Jan./Feb. 1966, pp. 121–125.

[6]Price, A. E., and Stallings, R. L., "Investigation of Turbulent Separated Flows in the Vicinity of Fin Type Protuberances at Supersonic Mach Numbers," NASA TN D-3804, Feb. 1967.

[7]Voitenko, D. M., Zubkov, A. I., and Panov, Y. A., "Influence of Mach Number on Flow in a Three-Dimensional Separation Region," *Moscow University Bulletin, Ser. I, Mathematics and Mechanics,* Vol. 23, No. 2, 1968, pp. 115–118.

[8]Uselton, J. C., "Fin Shock-Boundary Layer Interaction Tests on a Flat Plate with Blunted Fins at $M = 3$ and 5," Arnold Engineering Development Center TR-67-113, Arnold Air Force Station, TN, June 1967.

[9]Westkaemper, J. C., "Turbulent Boundary Layer Separation Ahead of Cylinders," *AIAA Journal,* Vol. 6, No. 7, 1968, pp. 1352–1355.

[10]Lucas, E. J., "Investigation of Blunt Fin-Induced Flow Separation Region on a Flat Plate at Mach Numbers 2.5 to 4.0," Arnold Engineering Development Center TR-70-265, Jan. 1971.

[11]Kaufman, L. G., Korkegi, R. H., and Morton, L. C., "Shock Impingement Caused by Boundary Layer Separation Ahead of Blunt Fins," Aeronautical Research Lab., ARL 72-0118, Wright-Patterson AFB, Dayton, OH, Aug. 1972.

[12]Dolling, D. S., Cosad, C. D., and Bogdonoff, S. M., "An Examination of Blunt Fin-Induced Flows," AIAA Paper 78-159, Jan. 1978.

[13]Dolling, D. S., Cosad, C. D., and Bogdonoff, S. M., "An Examination of Blunt Fin-Induced Shock Wave Turbulent Boundary Layer Interactions," AIAA Paper 79-0068, Jan. 1979.

[14]Winklemann, A. E., "Experimental Investigations of a Fin Protuberance Partially Immersed in a Turbulent Boundary Layer at Mach 5," Naval Ordnance Lab., NOLTR-72-33, Silver Springs, MD, 1972.

[15]Gillerlain, J. D., "Fin-Cone Interference Flowfield," AIAA Paper 79-0200, Jan. 1979.

[16]Young, F. L., Kaufmann, L. G., and Korkegi, R. H., "Experimental Investigation of Interaction between Blunt Fin Shock Waves and Adjacent Boundary-Layers at Mach Numbers 3 and 5," Aerospace Research Lab., ARL 68-0214, Wright-Patterson AFB, Dayton, OH, Dec. 1968.

[17]Özcan, O., and Holt, M., "Supersonic Separated Flow Past a Cylindrical Obstacle on a Flat Plate," *AIAA Journal,* Vol. 22, No. 5, 1984, pp. 611–617.

[18]Hung, C. M., and Kordulla, W., "A Time-Split Finite-Volume Algorithm for Three-Dimensional Flowfield Simulation," *AIAA Journal,* Vol. 22, No. 11, 1984, pp. 1564–1572. .

[19]Horstman, C. C., "A Computational Study of Complex Three-Dimensional-Compressible Turbulent Flowfields," AIAA Paper 84-1556, July 1984.

[20]Knight, D. D., "Modelling of Three-Dimensional Shock-Wave/Turbulent Boundary Layer Interaction," Workshop on Macroscopic Modelling of Turbulent Flows, Valbonne, France, Dec. 1984.

[21]Hung, C. M., and Bunning, D. G., "Simulation of Blunt-Fin-Induced Shock Wave and Turbulent Boundary-Layer Interaction," *Journal of Fluid Mechanics,* Vol. 154, May 1985, pp. 163–185.

[22]Knight, D. D., Horstman, C. C., Shapey, B., and Bogdonoff, S., "Structure of Supersonic Turbulent Flow Past a Sharp Fin," *AIAA Journal,* Vol. 25, No. 10, 1987, pp. 1331–1337.

[23]Baldwin, B. S., and Lomax, H., "Thin Layer Approximation and Algebraic Model for Separated Turbulent Flows," AIAA Paper 78-257, Jan. 1978.

[24]Hung, C. M., and Kurasaki, S. S., "Thin-Layer Approximation for Three-Dimensional Supersonic Corner Flows," *AIAA Journal,* Vol. 18, No. 12, 1980, pp. 1544–1546.

[25]Thomas, D. D., and Middlecoff, J. F., "Direct Control of the Grid Point Distribution in Meshes Generated by Elliptic Equations," *AIAA Journal,* Vol. 18, No. 6, 1980, pp. 652–654.

[26]MacCormack, R. W., "The Effect of Viscosity in Hypervelocity Impact Cratering," AIAA Paper 69-354, May 1969.

[27]Devenport, W. J., Agarwal, N. K., Dewitz, M. B., Simpson, R. L., and Poddar, K., "Effects of a Fillet on the Flow Past a Wing-Body Junction," *AIAA Journal,* Vol. 28, No. 12, 1990, pp. 2017–2024.